

MAIN TEXT

Durable scalable 3D SLA-printed cuff electrodes with high performance carbon + PEDOT:PSS-based contacts

Onna Marie Doering¹  | Christian Vetter¹  | Awadh Alhawwash^{2,3}  | M. Ryne Horn¹  | Ken Yoshida¹ 

¹Department of Biomedical Engineering, Indiana University – Purdue University Indianapolis, Indianapolis, Indiana, USA

²Weldon School of Biomedical Engineering, Purdue University, West Lafayette, Indiana, USA

³Biomedical Technology Department, King Saud University, Riyadh, Saudi Arabia

Correspondence

Ken Yoshida, Department of Biomedical Engineering, Indiana University – Purdue University Indianapolis, Indianapolis, IN, USA.
Email: yoshidak@iupui.edu

Funding information

National Institutes of Health, Grant/Award Number: R21EB028469

Abstract

Background: The stimulation and recording performance of implanted neural interfaces are functions of the physical and electrical characteristics of the neural interface, its electrode material and structure. Therefore, rapid optimization of such characteristics is becoming critical in most clinical and research studies. This paper describes the development of an upgraded 3D printed cuff electrode shell design containing a novel intrinsically conductive polymer (ICP) for stimulation and recording of peripheral nerve fibers.

Methods: A 3D stereolithography (SLA) printer was used to print a scalable, custom designed, C-cuff electrode and I-beam closure for accurate, rapid implementation. A novel contact consisting of a percolated carbon graphite base electrodeposited with an intrinsically conductive polymer (ICP), poly(3,4-ethylenedioxythiophene) polystyrene sulfonate (PEDOT:PSS) produced a PEDOT:PSS + carbon black (CB) matrix that was used to form the electrochemical interface on the structure. Prototype device performance was tested both in-vitro and in-vivo for electrical chemical capacity, electrochemical interfacial impedance, surgical handling, and implantability. The in-vivo work was performed on the sciatic nerve of 25 anesthetized Sprague Dawley rats to demonstrate recording and stimulating ability.

Results: Prototypes of different spatial geometries and number of contacts (bipolar, tripolar, and tetrapolar) were designed. The design was successfully printed with inner diameters down to 500 μm . Standard bipolar and tripolar cuffs, with a 1.3 mm inner diameter (ID), 0.5 mm contact width, 1.0 mm pitch, and a 1.5 mm end distance were used for the functional tests. This geometry was appropriate for placement on the rat sciatic nerve and enabled in-vivo testing in anesthetized rats. The contacts on the standard bipolar electrode had an area of $2.1 \times 10^{-2} \text{ cm}^2$. Cyclic voltammetry on ICP coated and uncoated graphite contacts showed that the ICP increased the average charge storage capacity (CSC) by a factor of 30. The corresponding impedance at 1 Hz was slightly above 1 k Ω , a 99.99% decrease from 100 k Ω in the uncoated state. The statistical comparison of the pre- versus

This is an open access article under the terms of the [Creative Commons Attribution-NonCommercial](https://creativecommons.org/licenses/by-nc/4.0/) License, which permits use, distribution and reproduction in any medium, provided the original work is properly cited and is not used for commercial purposes.

© 2022 The Authors. *Artificial Organs* published by International Center for Artificial Organ and Transplantation (ICAOT) and Wiley Periodicals LLC.



post-stimulation impedance measurements were not significantly different (p -value > 0.05).

Conclusions: The new cuff electrode enables rapid development of cost-effective functional stimulation devices targeting nerve bundles less than 1.0 mm in diameter. This allows for recording and modulation of a low-frequency current targeted within the peripheral nervous system.

KEYWORDS

3D printing, cuff electrode, electrode contact, improved charge transfer capacity, intrinsically conductive polymer

1 | INTRODUCTION

Neuromodulation through the application of electrical stimulation on target tissues elicits changes in the bioelectrical activity of the nervous system, thereby modulating organ or systemic function. Stimulation may be delivered in many forms, such as pulses, bursts, high-frequency alternating current (HFAC), and the recently developed, low-frequency alternating current (LFAC). Additive neural modulation actively induces neural activity, such as musculoskeletal stimulation, sensory stimulation, or a combination thereof. One example of musculoskeletal stimulation is functional electrical stimulation (FES) which activates motor units that innervate skeletal muscles, to induce functional contractions for musculoskeletal control.¹⁻⁷ Stimulation of nerve fibers with sensorized prosthetic limbs can evoke sensations through the amputated limb, providing neural traffic to induce plastic changes in the central nervous system, and redirect signals inducing phantom limb pain. Recording of sensory information, stimulated or organic, in a feedback loop can also trigger the stimulation of muscles in the corresponding pathway.⁸⁻¹²

Subtractive neural modulation, a lesser developed technique, aims to utilize electrical stimulation to reduce or block neural activity. A method under investigation in our lab is a subtractive stimulation modality using a continuous sinusoidal, LFAC, waveform delivered through an implanted circumferential cuff electrode. The waveform slows or completely blocks a conducting action potential at lower stimulus amplitudes, in a safe and reversible, charge balanced manner compared to other modalities.^{13,14} In comparison to the short duration impulses delivered by standard pulse stimulations, the LFAC waveform requires continuous delivery of the waveform at a cycle frequency between 0.5 and 10 Hz. Standard pulse stimulation can rely on the stored electrolyte double layer charge and non-Faradaic currents to sustain short duration currents. LFAC, however, requires electrodes capable of transmitting Faradaic currents to sustain a continuous ionic current.

Cuff electrodes have a long-standing research history and are among the most widely used neuromodulatory interfaces for peripheral nerve stimulation.^{1-5,15-21} They are applied directly around the nerve trunk and designed to direct electric currents within the nerve bundle. The physical and electrical characteristics of the neural interface, summarized as the electrode contact material and structure, play a key role in the device's stimulation and recording performance. The contact material plays a principal role in the interfacial impedance and charge transfer characteristics. Performance is strongly influenced by the interface's geometry, which includes the insulating structure, contact size, distribution, and symmetry.

Irrespective of the application, electrodes must be designed to safely provide therapeutic stimulation whereby electrical current, or its induced potential field, is capable of depolarizing excitable membrane tissue at the electrode-electrolyte interface. Conventional metal electrodes (CMEs), such as stainless steel or platinum used in early neural interfaces, adequately conduct current at high frequencies (>100 Hz).²²⁻²⁴ Low frequency behavior, characterized by high, largely reactive impedance in electrochemical impedance spectroscopy (EIS), makes it difficult to effectively pass currents through the electrode-electrolyte interface. The polarizability of the electrodes exhibiting these characteristics induces an electrochemical potential until the activation energy for a permissive electrochemical pathway is reached. Unfortunately, in aqueous environments, one such pathway is hydrolysis, which leads to the buildup of corrosive ionic species through the decomposition of water into hydrogen and hydroxide ions. Even at lower levels, development of these reaction species could elicit an immune response that leads to an increase in local impedance.^{24,25} The CME's electrical drawbacks can be diminished through careful selection of metals that are less polarizable, such as platinum or iridium-oxide, by use of intrinsically conductive polymers (ICP), or some combination thereof.

The effectiveness of the contact material operates in tandem with the structure's ability to provide an appropriate spatial organization for the targeted end use. With



the desire to advance the study of LFAC, *in-silico* models suggest that non-standard electrode geometries may minimize the potential needed to support the phenomenon.²⁶ A rapid means to implement prototype structures is needed to optimize the electrode geometry before a commercially manufacturable product is possible. High-resolution 3D stereolithography (SLA)-printing is a precise and highly reproducible technique that permits robust, rapid prototyping and testing while requiring less manufacturing time, cost, and equipment than silicone-based methods of similar geometry and precision.^{1,12,15,17,27,28} The previously reported hinge cuff was a 3D SLA-printed structure with precisely defined structure geometries and stainless-steel contacts (Figure 1A).²⁹ The methodology involved in the fabrication of the hinge cuff increased experimental throughput, but the design itself exhibited significant functional limitations. The most notable limitations were

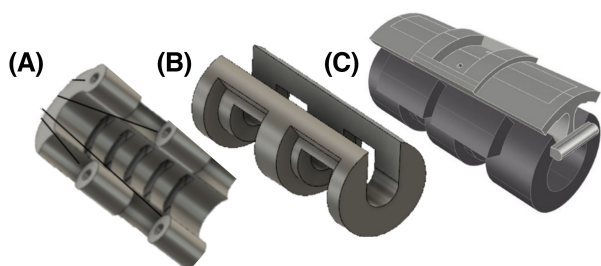


FIGURE 1 The 3D cuff design originated as the two-component hinge cuff (A), whose evolution was motivated by significant functional limitations including current leakage and electrical instability in the metal contacts. The next generation U-cuff (B) simplified the manageability of the electrode but required further optimization to address the remaining current leakage issues. The current C-cuff electrode design (C) includes an I-beam closure that addresses the functional limitations encountered in the previous designs.

the current leakage at the opening and hinge of the cuff, as well as the electrical instability of the stainless-steel contacts. The U-cuff (Figure 1B), an intermediate successor to the hinge cuff, addressed the hinge current leakage and wire management issues but required further design changes to fulfill the requirements for LFAC studies.

In the present study we developed the C-cuff (Figure 1C), novel in both its structural design and contact material, which addresses the limitations of previous 3D printed cuff electrode designs. The structure is functionally enhanced by the inclusion of an I-beam closure that provides the complete circumferential insulation that was missing in its predecessors. Contact stability is improved by introducing an ICP contact material that exhibits improved charge transfer characteristics and reduced impedance in a low frequency band. This resultant structure allows a broad range of non-standard geometries to be studied rapidly with an electrode that is electrochemically stable and able to effectively record neural signals and deliver LFAC. To verify the functional stimulating and recording performance of the cuff design, two prototype models were tested in-vivo.

2 | METHODS

2.1 | 3D printed design

The cuff and closure base designs and modifications were modeled using computer-aided design (CAD) software (AutoCAD 2022, Autodesk, San Rafael, CA, USA) for implantation optimization and experimental aim. All cuff shells, regardless of inner diameter, are C-shaped cylinders that cover approximately 80 percent of the nerve circumference and have a wall thickness of 500 μm (Figure 2). The contact face is inset 250 μm from the inner diameter,

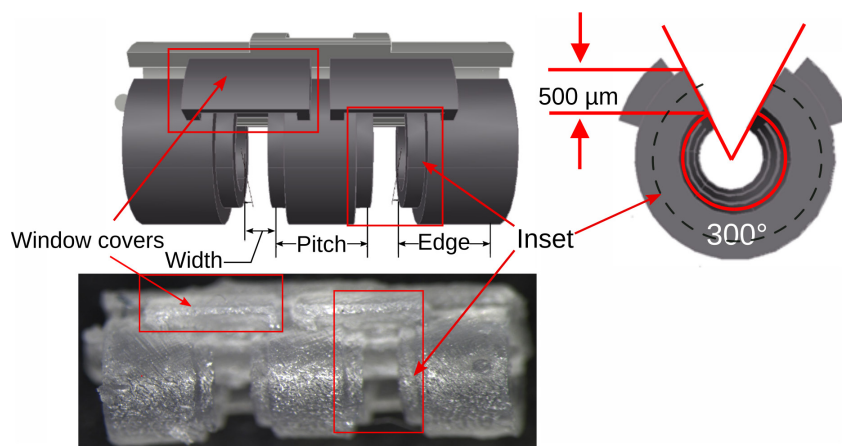


FIGURE 2 The new C-cuff shell, designed in CAD, features an overall wall thickness of 500 μm , 250 μm inset windows, 300° circumferential nerve-electrode interface coverage, and window covers that have optimized the functionality of the cuff in-vivo. ID, contact number, contact width, contact pitch, and contact edge-to-end distance are scalable factors of interest. [Color figure can be viewed at wileyonlinelibrary.com]

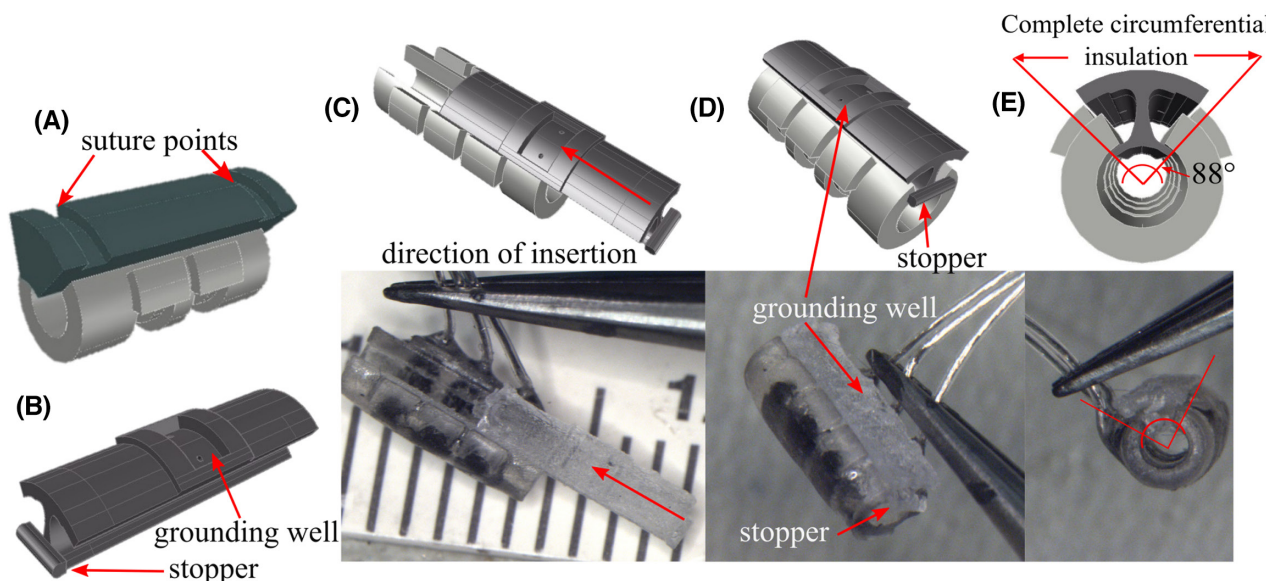


FIGURE 3 The initial wedge closure design (A) was modified to the I-beam closure (B) which eliminated the need for sutures and provided a stopper for functionality and an optional grounding well. The I-beam slides along the length of the cuff (C) until the stopper (D) reaches the outside edge of the cuff, holding it in place. The design overlap prevents structure slip and current leakage (E) covering 88° circumferentially. [Color figure can be viewed at wileyonlinelibrary.com]

central to the wall thickness. Additionally, insets are open to the backside of the cuff, creating windows to precisely define the contact surface and wire locations. This prevents contact-to-contact shunting down the length of the cuff. Window covers, at the ends of the windows and on the backside of the cuff, assist with wire placement during the assembly process. The base design is capable of scaling inner diameter (ID), contact number, contact width, contact pitch, and contact edge-to-end distance to optimize cuff geometries for the specific research aims.

The initial closure structure was a wedge (Figure 3A) that fit into the opening of the cuff to provide complete insulation around the nerve via structural means. Two grooves on the top face of the wedge were added as suture points to secure it in place during implantation. The wedge closure was modified into the novel design of the I-beam closure (Figure 3B). This closure spans the length of the cuff, with a stopper at one end to prevent slide-through during implantation (Figure 3C). The well at the top of the beam serves as an optional grounding point at an isopotential line (Figure 3D). The inner surface of this closure overlaps and sits flush with the cuff shell to insulate the remaining 20 percent of the nerve circumference (Figure 3E).

2.2 | 3D printing

Stereolithography (STL) files of 3D cuff and I-beam designs were generated and used in the 3D printer software (Preform 3.2.2, Formlabs Inc., Somerville, MA, USA) to print the design. Structures were positioned at a 30-degree

angle, horizontal with the cuff opening upward to allow for proper media drainage during printing. Cuffs were printed on an SLA 3D printer (Form 2, Formlabs Inc., Somerville, MA, USA) using clear photopolymer resin (FLGPCL04, Formlabs Inc., Somerville, MA, USA) and rinsed in isopropyl alcohol upon print completion. Excess media was removed before curing in a heated ultraviolet (UV) cure chamber (Form Cure, Formlabs Inc.) at 60°C for 20 min.

2.3 | Electrode contact and cuff assembly

To assemble a functional cuff, the shell was first placed on a hypodermic needle and the exposed contact surface windows were masked with silicone from the inner diameter surface to the inset edge. Wires were then added through the window covers (Figure 4A) and pulled taut after filling the windows flush to the back surface of the cuff shell with the composite contact paste. The paste consisted of cyanoacrylate with sufficient carbon graphite to reach the percolation threshold and yield a conductive paste (Figure 4B). After the contact paste was air dried, the contacts and wires were insulated on the backside of the cuff with print media and UV cured (Figure 4C). Following initial fabrication, the novel ICP consisting of 3,4-Ethylendioxythiophene (EDOT) and polystyrene sulfonate (PSS) in a carbon black (CB) suspension was oxidatively electropolymerized on the electrode contacts. This resulted in a poly(3,4-ethylendioxythiophene) polystyrene sulfonate (PEDOT:PSS)+CB matrix that formed the electrochemical interface on the contacts of the structure.

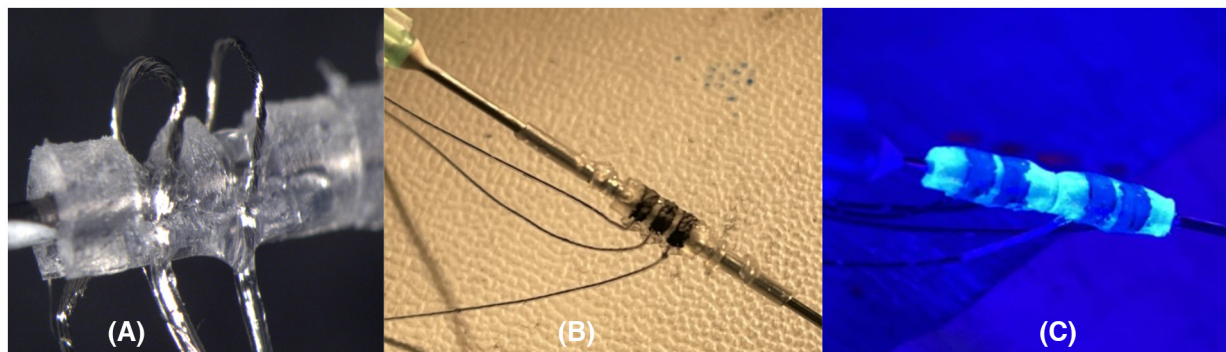


FIGURE 4 Cuff assembly. (A) Wires are added through the cuff windows. (B) Contact paste is added to the windows and wires are pulled through such that the paste is flush with the edge. (C) after air drying, the contacts are insulated in media and UV cured. UV curing is the last step of the initial construction process. [Color figure can be viewed at wileyonlinelibrary.com]

The final structure was stored for experimental use in a sealed, nitrogen-rich bag to prevent oxidation.

2.4 | Electrochemical analysis

A more comprehensive treatment of the electrochemical interface can be found in work conducted by Vetter.²⁵ Application of that interface into a functional electrode is described above, and a brief description of the electrochemical analysis is as follows. The electrochemical analysis consisted of electrochemical impedance spectroscopy (EIS) and cyclic voltammetry (CV) of the contact within the cuff structure. The CV was acquired using a sweep-rate (SR) of 4000 mV/s. Additionally, measurements were made at two separate points: (1) before and (2) after the electrodeposition of the PEDOT:PSS + CB ICP. All depositions and measurements were made using an electrochemical interface (SI1287, Solartron Analytical, Berkshire UK). EIS and CV were also performed within a phosphate buffer saline solution (PBS) (Gibco™ PBS, Thermo Fisher Scientific, Grand Island, NY, USA) at pH 7.4, and an additional CV was performed after deposition with a SR of 50 mV/s. The cathodic charge storage capacity (CSC) was calculated using custom-written software in MATLAB (Matlab 2020b, The Mathworks, Natick MA, USA).

2.5 | In-vivo surgical implantation and testing

All animal care and experimental procedures were approved by the School of Science Institutional Animal Care and Use Committees (IACUC) of Indiana University-Purdue University Indianapolis. Acute experiments were performed on 25 adult Sprague Dawley rats, and preliminary results and detailed surgical procedures were presented elsewhere.³⁰ Animals were sedated and

anesthetized with inhalation of isoflurane and maintained a 1.5%–2.0% isoflurane dose via nose cone with an oxygen flow rate of 2.0 L/min. The left hindlimb was shaved, and surgical access to the sciatic nerve was obtained through an incision was made at the posterior mid-thigh level. Blunt dissection was used to expose the sciatic nerve trunk through the branches at the popliteal fossa. The animal was placed in a prone position and its left foot was securely attached to the pedal of a force transducer system (300C, Aurora Scientific, Aurora, ON, Canada). The body temperature was monitored via rectal thermometer and maintained at ~37.5°C over a heating pad and a 100 W Edison bulb, as necessary. Non-invasive measurements of tail blood pressure, heart rate, and oxygen saturation were monitored throughout the experiment.

Two cuff electrodes were implanted for this experimental setup (Figure 5). A bipolar cuff electrode was implanted on the sciatic nerve most proximal, for pulse stimulation. A tripolar cuff electrode, implanted on the tibial branch of the sciatic nerve most distal, was used for electroneurograph (ENG) signal recording. The common peroneal (CP) was crushed through suture ligation to eliminate dorsiflexor muscle responses prior to stimulation and recording protocols. Muscle twitches were evoked by monophasic rectangular pulses presented to the bipolar cuff with a pulse-width of 100 μs at 1 Hz frequency. The stimulus strength was increased gradually, and each strength was applied for at least 10s with a 5 s resting period between each increment. The stimuli were delivered using an optoisolated stimulator (DS3, Digitimer LTD, Hertfordshire UK) triggered by an arbitrary pulse generator (Analog Discovery 2, Digilent Inc, Pullman WA) and controlled via a custom written LabVIEW® software. ENG signals were measured by the tripolar cuff electrode using a true-tripolar measurement. Intramuscular electromyography (EMG) signals were measured using stainless steel wires (Cooner wire, Chatsworth, CA) placed within the triceps surae muscle. Both signals were amplified in

In-vivo Experimental Setup and Electrodes Placement

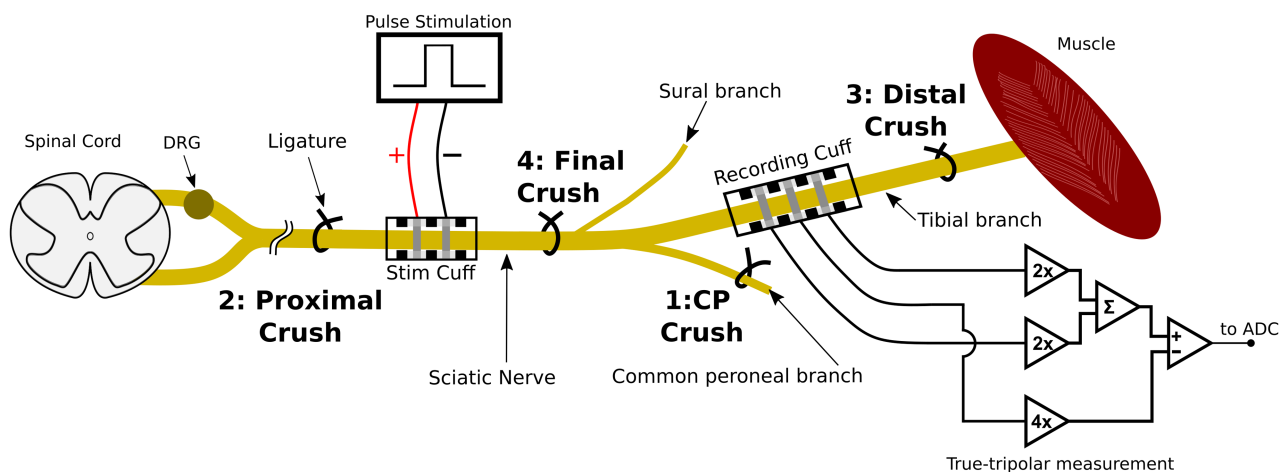


FIGURE 5 Illustration of the experimental setup and electrodes placement. A bipolar cuff electrode was placed most proximal and used for pulse stimulation. A tripolar cuff was placed most distal, used for ENG recording. The CP crush was performed during the surgery. Subsequent control crushes were performed during the experiment. [Color figure can be viewed at wileyonlinelibrary.com]

different channels using a variable gain universal invertible amplifier (UIA 3.7, Yoshida, 2021).³¹

To evaluate and assess the electrode's functionality in terms of stimulation and recording, recruitment curves of muscle twitches were collected with simultaneous recordings of the ENG signal with different stimuli strengths. To verify interpretation of the various peaks in the ENG recordings, the nerve was sequentially crushed at various levels using surgical ligation followed by repetition of the ENG measurement protocol (Figure 5). The crushes aimed to eliminate various components of the stimulus response by disrupting action potential conduction as follows: (1) Proximal crush eliminated spinal reflex responses, (2) Distal crush eliminated the direct muscle response without disrupting the compound nerve action potential (CNAP), (3) Final crush eliminated the CNAP. All signals were recorded with a sampling rate of 48 kHz (HD24, Alesis, Cumberland, RI, USA).

Following implantation of the electrodes, complex impedance of the stimulating electrode contacts was characterized using the rapid impedance measurement technique.³² The effect of stimulation on the electrode was characterized by the repetition of the measurements at the end of the experiment. Each impedance measurement was taken as a two-point measurement to show the full-cell characterization using a sampling rate of 500 kHz (National Instruments-DAQ).

2.6 | Data analysis of in-vivo measurements

All acquired data were processed in MATLAB® (Matlab 2020b, The Mathworks, Natick MA, USA). EMG signals

were zero-meaned and digitally filtered with a bandpass filter from 300 Hz to 3 kHz. Recruitment curves of the evoked muscle twitches were calculated based on the average peak-to-peak values of twitches during 10 s of stimulation for each stimuli strength. Due to variations in the animals' conditions, the recruitment curves were normalized to the maximum value. Then a sigmoidal curve fit³³ was applied to determine the motor threshold, defined as a 5% increase from the baseline. The recruitment curves were then normalized in terms of currents to the 5% motor threshold. The raw ENG signals were zero-meaned and used to identify the CNAP using spike-triggered averaging within a 10 ms window. The subsequent datasets were compared against the control cases to show changes in the CNAP recordings and the separation of muscle activity (EMG pickup) from the CNAP within the ENG recording.

Complex impedance measurements were analyzed in terms of magnitude and phase for frequencies between 0.2 Hz to 100 kHz. The mean and standard deviation were calculated to compare impedance changes prior to and following pulse stimulation. Due to technical issues, only 24 measurements were considered in this analysis. The measurements of the impedance magnitude and phase pre- and post-stimulation were compared statistically at each frequency using paired student *t*-test ($\alpha = 0.05$).

3 | RESULTS

3.1 | Design

These cuffs have been successfully printed with varying spatial geometries (Figure 6A–C) and contact numbers

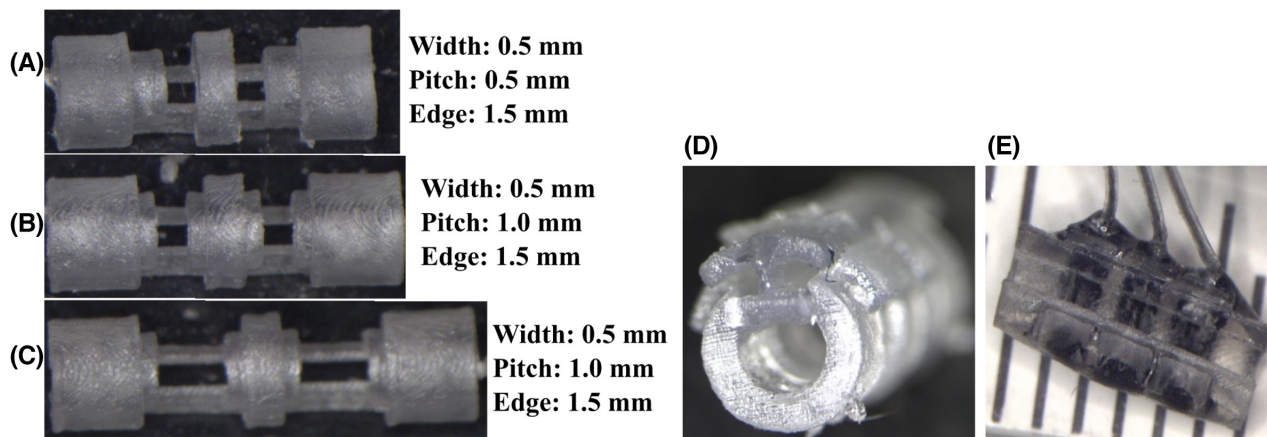


FIGURE 6 (A–C) printed 650 μm ID bipolar C-cuff electrodes with varying spatial geometries. (D) the I-beam is shown seated at the face of a C-cuff, which prevents slide-through during implantation. The bipolar cuff electrode shell and I-beam closure are friction-held together, reducing suture requirements. (E) a completely constructed tripolar C-cuff highlighting the carbon graphite contacts within the shell.

to include bipolar (Figure 6D), tripolar (Figure 6E), and tetrapolar versions. 500 μm is the smallest successful inner diameter to be fabricated with this design and technique. The standard geometry for the rat sciatic models was a 1.3 mm ID, 0.5 mm contact width, 1.0 mm pitch, and a 1.5 mm end distance. The I-beam closure functions as intended to secure the cuff around the nerve and to provide total circumferential structural insulation (Figure 6D).

3.2 | Electrochemical analysis

The percolated carbon graphite contacts, with an area of $2.1 \times 10^{-2} \text{ cm}^2$, had a cathodic CSC of -22.11 mC and -47.52 mC prior to coating. This was increased to -805.3 mC and -1108 mC following ICP deposition (SR = 4000 mV/s). The impedance at 1 Hz prior to deposition was $2.636 \times 10^6 \Omega$ (-33.64° phase) and $3.075 \times 10^5 \Omega$ (-62.92° phase) which was decreased to 1448Ω (-11.59° phase) and 1463Ω (-16.80° phase) following ICP deposition (Figure 7). In both cases, the impedance reached R_∞ at low frequencies ($<10 \text{ Hz}$). The additional CV performed after electrodeposition (SR = 50 mV/s) had a cathodic CSC of $-623.6 \text{ mC}\cdot\text{cm}^{-2}$.

3.3 | Surgical

Various iterations of the device were successfully implanted on the sciatic nerve, between the sciatic notch and the popliteal fossa, of 25 Sprague–Dawley rats. The I-beam closure fit precisely within the cuff opening and offered a physical barrier that kept the nerve in place without additional sutures (Figure 8). Compared to previous hinge closures, this design further decreased the time needed

for implantation with less cable management and moving structure to work with. At the end of each experiment, the coated cuffs were cleaned and stored in beakers filled with ddH₂O until they were reused for another terminal experiment. Once the nerve was exposed, implantation and fixation of the C-cuff with I-beam closure took less than five minutes.

3.4 | In-vivo functionality

The C-cuff electrodes were able to repeatedly stimulate the sciatic nerve and evoke muscle twitches with varying strengths of stimuli (Figure 9). Although the maximum value of the twitches was different in magnitude between animals, the normalized recruitment curves demonstrate the repeatability of the stimulation scheme. The fit of the cuff was adequately sized for the nerve diameter range as the variation in motor thresholds ($186.36 \pm 27 \mu\text{A}$) was minimal using the same pulse width of 100 μs . In the representative example of the cuff electrode recording, the CNAP was shown at multiple stimulation strengths following each of the controlling nerve crushes (Figure 10). The post CP crush recordings shows the initial stimulation results after implantation, where the evoked CNAP was $<2 \text{ ms}$ after the stimulus artifact (Figure 10A). Similarly, the proximal crush, which was meant to eliminate the spinal reflex activity, confirms stimulation affects only the motor pathway to evoke muscle twitches (Figure 10B). Both Figure 10A,B show the CNAP but contain significant contamination from the EMG signal. The distal crush was able to eliminate the EMG signal such that only the CNAP was shown (Figure 10C). The final crush between the stimulating and recording electrode eliminated the CNAP from the recording by disrupting the evoked action

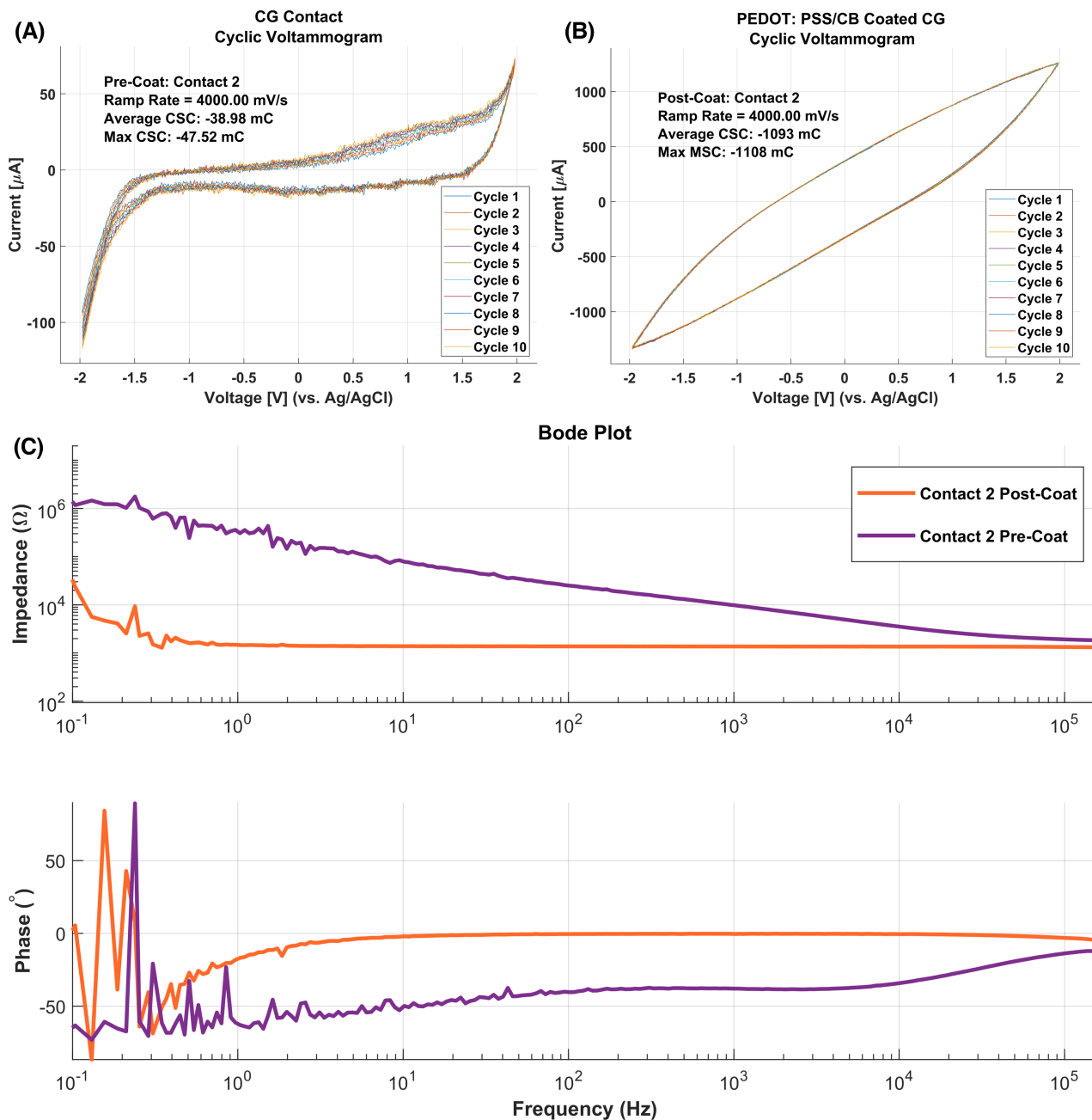


FIGURE 7 Cyclic voltammogram and the corresponding electrochemical impedance spectrogram of the carbon graphite contact before (A) and after PEDOT:PSS+CB coating (B). (C) shows the corresponding EIS of the contact before and after coating. Before coating, the contact is mostly reactive in the bandwidth relevant to neural stimulation, recording and LFAC stimulation (0.5 Hz–20 kHz). This becomes resistive after coating indicating improved interfacial conductivity. [Color figure can be viewed at wileyonlinelibrary.com]

potential valley before it reaches the recording electrode (Figure 10D). This provided experimental proof that the signal recorded was the conducted CNAP. The statistical comparison of the in-vivo complex impedance measurements of the stimulating electrodes were not significantly different (p -value > 0.05) (Figure 11), even though each experiment lasted more than 6 h, and each electrode delivered 7000 to 10 000 pulses during each experiment. Therefore, these in-vivo impedance measurements demonstrated that the cuff and its contacts were operating within safe and stable functional ranges.

4 | DISCUSSION

This work presents the C-cuff, the latest incarnation of our custom 3D printed cuff electrodes. These robust, easily fabricated, and user-friendly electrodes overcame several limitations of previous designs. In prior work, we introduced the 3D printed hinge and U-cuffs. The hinge cuff structurally confined experiments to larger targeted nerves since the 3D printer resolution limited the inner diameter and wall thickness to sizes that supported hinge patency. This lab's research aims required structures that

work with smaller nerve bundles at or below 1 mm in diameter. Complicating matters, each contact in this cuff design was split by the halves of the hinge, requiring two wires to enable a connection. Furthermore, the inclusion of the hinge limited the contact surface area to approximately 50% of the nerve circumference where 75% coverage was preferred.¹

The U-cuff resolved the electrode contact and wiring problem by removing the hinge and replacing the two-facet contacts to a continuous stainless-steel contact plate. This eliminated the current leakage along the hinge, simplified implantation wire management, and moderately

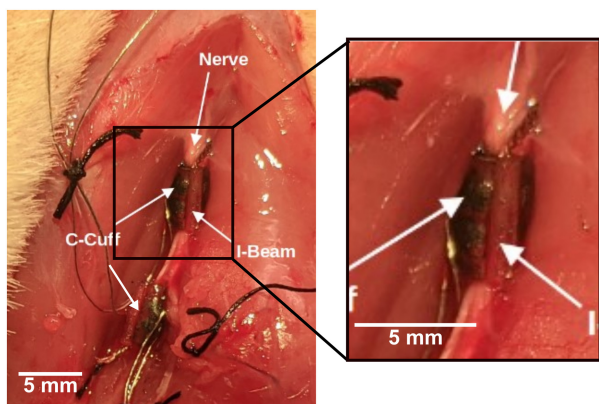
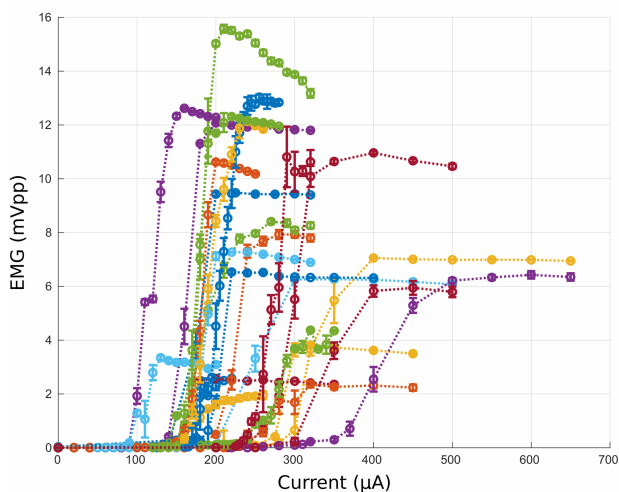


FIGURE 8 The C-cuffs with I-beam closures were implanted between the popliteal fossa and the sciatic notch of rat models. This serves to demonstrate the spatial relativity of the entire constructed electrode (cuff and I-beam) to the implantation site and the nerve. [Color figure can be viewed at wileyonlinelibrary.com]

increased the contact surface area coverage. The open side of the U-cuff enabled placement of the nerve within the cuff structure but left a large uninsulated portion of the nerve either exposed to air or physiological solution. A mineral oil bath applied to the implantation site offered a temporary solution for acute studies where surgical access was kept open. A permanent structural means to completely insulate the cuff and prevent the contact-to-contact shunt path needed to be implemented for translation to a closed site or chronic application. As a result, inset contact windows on the backside of the cuff shell were designed to create a larger surface area for contact placement. The stainless-steel contacts were manually cut, and the inset allowed for natural dimensional deviations while standardizing the inward facing exposed contact surface area. The secondary function of the inset was to direct glue away from the contact surface. This would ideally prevent surface fouling during fabrication and produce a clean electrically conductive surface. Overall, the U-cuff failed to provide adequate support or protection during the assembly process and required further design optimization.

The novel C-cuff design addressed the limitations of the U-cuff and hinged cuff designs. The C-cuff's windows, adapted from the U-cuff, precisely outlined the contact area by creating a well to hold the carbon-graphite contact paste. The addition of window covers secured and fully embedded the wires within the carbon-graphite paste before curing. This process consequently created a larger contact surface area on the back of the cuff compared

(A) Experimental EMG Recruitment
PW=100 μ sec, N=25



(B) Normalized EMG Recruitment
PW=100 μ sec, N=25

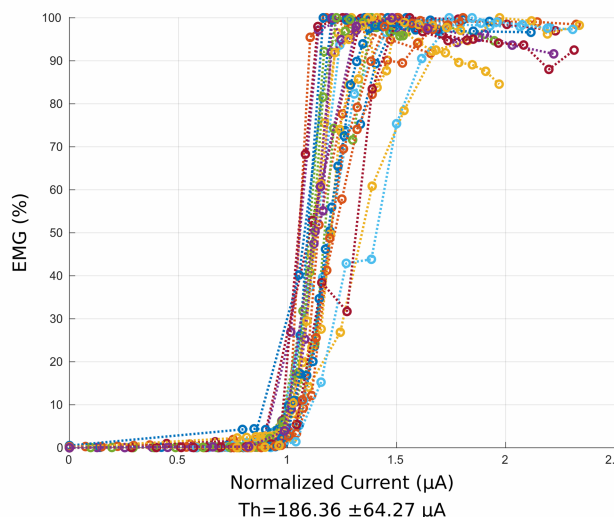


FIGURE 9 EMG peak-to-peak recruitment curves during pulse stimulation through the bipolar cuff of 25 experiments using 100 μ s pulse width at 1 Hz frequency. (A) Experimental average peak-to-peak values during 10s of stimulation (error bars are standard deviation). (B) the recruitment curve magnitudes were normalized to the maximum value of each experiment. Currents were normalized to the estimated 5% motor threshold of each experiment. [Color figure can be viewed at wileyonlinelibrary.com]

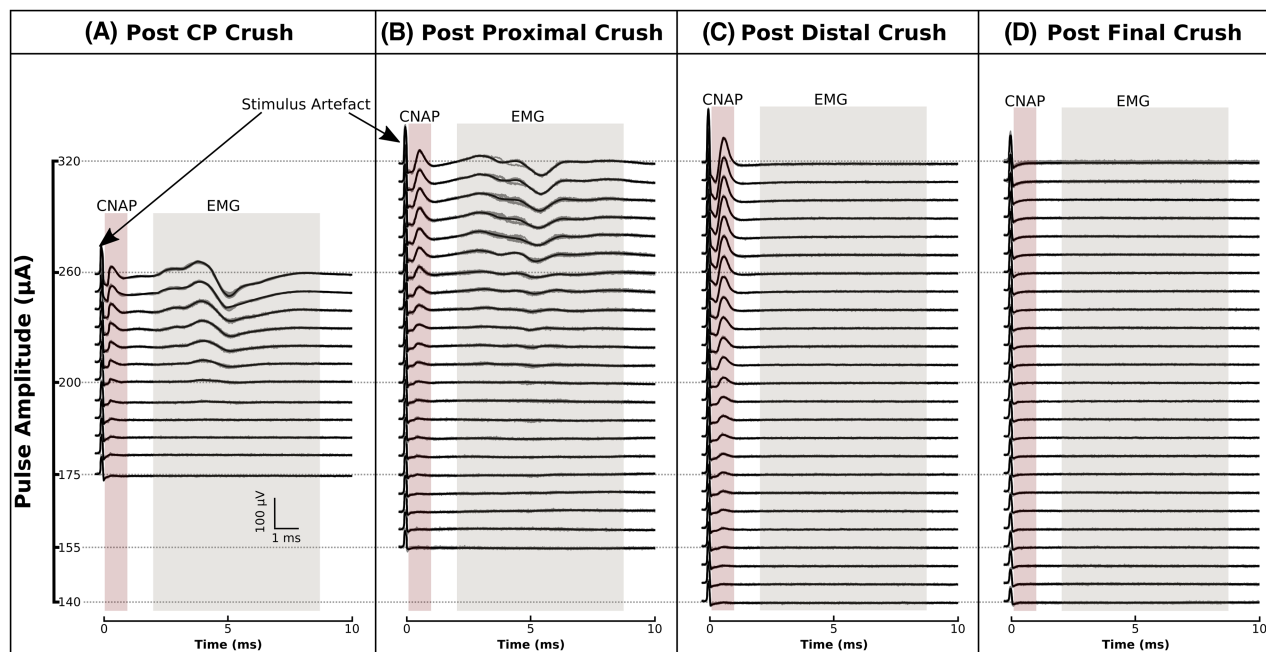


FIGURE 10 A representative example (rat number C20613) demonstrating the ability of the tripolar cuff electrode to record the CNAP extracted from the ENG spike-triggered averages (in a 10 ms window) during multiple experimental and control runs. (A) Initial results of ENG spike-triggered averages following CP crush. (B) the ENG spike-triggered averages following proximal crush. (C) the ENG spike-triggered averages following distal crush showing the elimination EMG components. (D) the ENG spike-triggered averages following final crush between the bipolar stimulating cuff and the tripolar recording cuff showing the absence of conducting CNAP. The CNAP region is shaded <2 ms following the stimulus artifact in each panel followed by the EMG region. Each trace shows the average (black) of at least 10 pulses (gray traces). [Color figure can be viewed at wileyonlinelibrary.com]

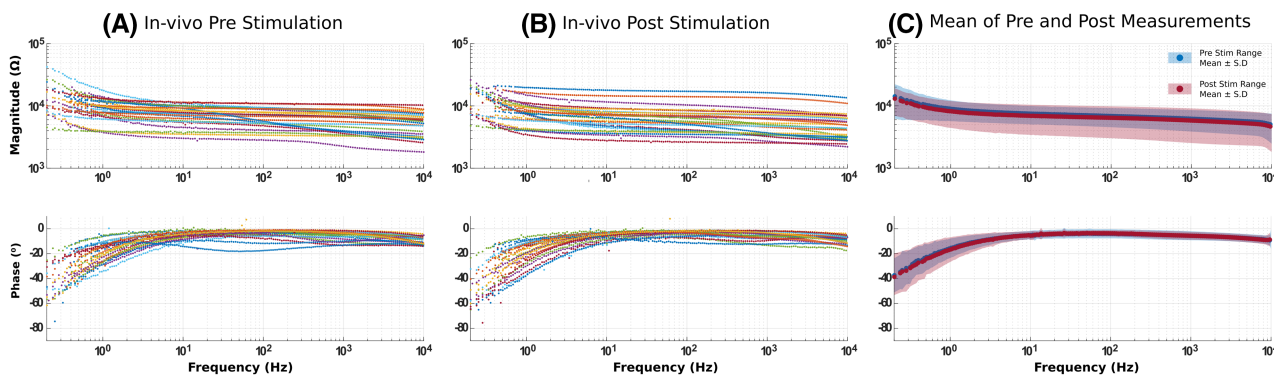


FIGURE 11 Complex impedance measurements ($N = 24$) of the bipolar stimulating cuffs in-vivo prior to and post stimulation. (A) the impedance magnitude and phase prior to stimulation (B) post stimulation, and (C) mean and ranges of standard deviation of pre and post stimulation showing the overlap. [Color figure can be viewed at wileyonlinelibrary.com]

to the smaller, well-defined surface areas at the contact-tissue interface. The result was a current concentration gradient that directs the current density toward the inside of the cuff, improving the current concentration at the electrode-nerve interface.

Properties of the carbon-graphite contacts are similar to CMEs showing an impedance where reactance becomes dominant below 1 kHz and resistive at frequencies $> \sim 1$ kHz. As such, sourcing currents for waveforms that are predominantly composed of high frequency

components, such as a traditional rectangular pulse stimulation, is generally possible within the linear region of the electrode. However, any bias currents or the DC offset current are magnified by the low-frequency impedance. This can lead to offset instabilities during recordings and/or electrode polarization during stimulation. It is particularly problematic when attempting to use CMEs to effect LFAC block or DC block. The results show that the novel PEDOT:PSS + CB ICP allowed for improved charge transfer in low frequencies during our relatively short



experiments (lasting ~10 h). The impedance at 10 Hz remained predominantly resistive in character and consistent with the impedance at higher frequencies (>1 kHz), indicating R_{∞} reached down to lower frequencies. These results show that the coating may be effective across all frequencies required for clinical neuromodulation, including new techniques such as LFAC and neural recordings. Ultimately, the use of this design (cuff and ICP contact) allowed for cost savings of more than 4000 times and a performance improvement in CSC of nearly 25 times to similar electrodes widely used for low frequency modulation. The standard cuff used to compare functional market equivalents was the 500 μm bipolar cuff (CorTec GmbH, Freiburg, Germany) with PEDOT-coated platinum contacts (Amplicot[®], Heraeus Medical Components, Saint Paul MN). The calibrated impedance of this device was 47 k Ω at 100 Hz and 16 k Ω at 1 kHz.

The resulting structure took less time to produce, and had substantial material cost savings without sacrificing durability, performance, or quality. Thinner walls in the electrode shell optimized the spatial availability at the implantation site compared to the hinge counterpart. By taking advantage of the anticlastic mechanical properties of the nerve under tension, the opening of the cuff was reduced from 180 degrees to 60 degrees while maintaining the same inner diameter. During implantation, the nerve was only stretched enough to fit inside the opening of the cuff to not cause tissue damage. Once inside the C-cuff, the nerve returned to its original diameter, reducing the likelihood of cuff dislocation before the I-beam closure was secured. Increasing the shell's circumferential coverage from 50% to 80% increased the available contact coverage to approximately 75% of the inner diameter compared to less than 50% in the U-cuff.

The initial wedge closure design provided the desired circumferential insulation but required sutures to hold it in place. This design was concerning because the sutures could come loose during the experiment, slip down around the nerve, and cause damage from ligation. The innovation from the wedge to the I-beam for a structural closure solved the issue of current leakage and resolved the concerns of unintended suture damage. This I-beam was friction-held and sat flush against both the inner surface and the opening of the cuff. With the I-beam covering the residual 20% of the circumference plus an additional 2.5% on each side of the opening, the permanent structural insulation problem was resolved.

The use of CAD software and 3D printing has provided the ability to make rapid modifications and improvements to the designs of both cuff and closure as needed. Customizable spatial changes in contact geometry as well as changes to contact number, amplified the number of test variables available for optimization. Further, 3D printing has provided an accurate way to repeatedly reproduce successful designs

in bulk. Having an inventory of blank shells and I-beams also eliminated the lag time for single component fabrication or third-party outsourcing. Our current research goals require customization of structures to non-standard dimensions and designs. Locally printing and manufacturing the structures and ICP carbon graphite contacts enabled rapid, reproducible production of prototype devices which immeasurably reduced cost and time. The volumetric throughput of realized product was only limited by the time it takes to handcraft these devices. The use of biocompatible 3D print media and more compliant structures need to be explored before translating the technique to a chronic solution and ultimately to applications in the medical arena.

AUTHOR CONTRIBUTIONS

Drafting and editing the manuscript, design and modification of the C-Cuff electrode: Onna Marie Doering. *Drafting and editing the manuscript, development and characterization of the Electrode PEDOT:PSS/CB ICP contact, and analysis of data:* Christian Vetter. *Drafting the R2 edits, running experimental protocols and analysis of data:* Awadh Alhawaash. *Running experimental protocols and analysis of data:* M. Ryne Horn. *Concept/Design of the C-Cuff electrode and PEDOT:PSS/CB ICP contact, grant funding to undertake study, management and administration of the project, drafting and editing of the manuscript:* Ken Yoshida.

ACKNOWLEDGMENTS


This work was funded by a grant from the National Institutes of Health (Trailblazer R21 grant R21EB028469). The authors acknowledge the IUPUI University Graduate Fellowship program for Ms. Doering's research fellowship. The authors also acknowledge support from the Familien Hede-Nielsens Fonden which enabled purchase of the 3D SLA printers used in this project.

CONFLICT OF INTEREST

The authors submitted an invention disclosure to the technology innovation office at the University.

ORCID

Onna Marie Doering  <https://orcid.org/0000-0001-9592-174X>

Christian Vetter  <https://orcid.org/0000-0002-2621-5611>

Awadh Alhawaash  <https://orcid.org/0000-0003-0044-5416>

M. Ryne Horn  <https://orcid.org/0000-0002-1066-6303>

Ken Yoshida  <https://orcid.org/0000-0003-4566-580X>

REFERENCES

1. Struijk JJ, Thomsen M, Larsen JO, Sinkjaer T. Cuff electrodes for long-term recording of natural sensory information. *IEEE Eng Med Biol Mag.* 1999 Jun;18(3):91–8.



2. Haugland MK, Hoffer JA, Sinkjaer T. Skin contact force information in sensory nerve signals recorded by implanted cuff electrodes. *IEEE Trans Rehabil Eng.* 1994 Mar;2(1):18–28.
3. Sinjkær T, Hinge B, Jørgensen A, Jensen ML, Haugland M. Whole sensory nerve recordings with spiral nerve cuff electrode. In: 1992 14th Annual International Conference of the IEEE Engineering in Medicine and Biology Society. Paris: IEEE; 1992. p. 1330–1331.
4. Crago PE, Peckham PH, Mortimer JT, Van Der Meulen JP. The choice of pulse duration for chronic electrical stimulation via surface, nerve, and intramuscular electrodes. *Ann Biomed Eng.* 1974 Sep;2(3):252–64.
5. Stein RB, Charles D, Hoffer JA, Arsenault J, Davis LA, Moorman S, et al. New approaches for the control of powered prostheses particularly by high-level amputees. *Bull Prosthet Res.* 1980;10–33:51–62.
6. Popovic DB, Stein RB, Jovanovic KL, Dai R, Kostov A, Armstrong WW. Sensory nerve recording for closed-loop control to restore motor functions. *IEEE Trans Biomed Eng.* 1993 Oct;40(10):1024–31.
7. Menezes IS, Cohen LG, Mello EA, Machado AG, Peckham PH, Anjos SM, et al. Combined brain and peripheral nerve stimulation in chronic stroke patients with moderate to severe motor impairment. *Neuromodulation.* 2018 Feb;21(2):176–83.
8. Ortiz-Catalan M, Mastinu E, Sassu P, Aszmann O, Brånemark R. Self-contained neuromusculoskeletal arm prostheses. *N Engl J Med.* 2020 Apr 30;382(18):1732–8.
9. Mastinu E, Ahlberg J, Lendaro E, Hermansson L, Håkansson B, Ortiz-Catalan M. An alternative myoelectric pattern recognition approach for the control of hand prostheses: a case study of use in daily life by a Dysmelia subject. *IEEE J Transl Eng Health Med.* 2018;6:1–12.
10. Middleton A, Ortiz-Catalan M. Neuromusculoskeletal arm prostheses: personal and social implications of living with an intimately integrated bionic arm. *Front Neurobot* [Internet]. 2020 [cited 2022 Feb 14];14:39. Available from: <https://www.frontiersin.org/article/10.3389/fnbot.2020.00039>
11. Raspopovic S, Valle G, Petrini FM. Sensory feedback for limb prostheses in amputees. *Nat Mater.* 2021 Jul;20(7):925–39.
12. Tyler DJ, Durand DM. Functionally selective peripheral nerve stimulation with a flat interface nerve electrode. *IEEE Trans Neural Syst Rehabil Eng.* 2002 Dec;10(4):294–303.
13. Muzquiz MI, Mintch L, Horn MR, Alhawwash A, Bashirullah R, Carr M, et al. A reversible low frequency alternating current nerve conduction block applied to mammalian autonomic nerves. *Sensors.* 2021 Jul 1;21(13):4521.
14. Muzquiz MI, Richardson L, Vetter C, Smolik M, Alhawwash A, Goodwill A, et al. In-vivo application of low frequency alternating currents on porcine cervical vagus nerve evokes reversible nerve conduction block. *Bioelectron Med.* 2021 Dec;7(1):9.
15. Stein RB, Charles D, Davis L, Jhamandas J, Mannard A, Nichols TR. Principles underlying new methods for chronic neural recording. *Can J Neurol Sci.* 1975 Aug;2(3):235–44.
16. Sinkjaer T. Integrating sensory nerve signals into neural prosthesis devices. *Neuromodulation.* 2000 Jan 1;3(1):33–41.
17. Naples GG, Mortimer JT, Scheiner A, Sweeney JD. A spiral nerve cuff electrode for peripheral nerve stimulation. *IEEE Trans Biomed Eng.* 1988 Nov;35(11):905–16.
18. Riso RR, Mosallaie FK, Jensen W, Sinkjaer T. Nerve cuff recordings of muscle afferent activity from tibial and peroneal nerves in rabbit during passive ankle motion. *IEEE Trans Rehabil Eng.* 2000 Jun;8(2):244–58.
19. Sinkjaer T, Haugland M, Struijk J, Riso R. Long-term cuff electrode recordings from peripheral nerves in animals and humans. In: Windhorst U, Johansson H, editors. *Modern techniques in neuroscience research* [Internet]. Berlin, Heidelberg: Springer; 1999. p. 787–802. https://doi.org/10.1007/978-3-642-58552-4_29
20. Veraart C, Grill WM, Mortimer JT. Selective control of muscle activation with a multipolar nerve cuff electrode. *IEEE Trans Biomed Eng.* 1993 Jul;40(7):640–53.
21. Stein RB, Nichols TR, Jhamandas J, Davis L, Charles D. Stable long-term recordings from cat peripheral nerves. *Brain Res.* 1977 Jun 3;128(1):21–38.
22. Yoshida K, Struijk JJ. *The theory of peripheral nerve recordings.* River Edge, NJ: World Scientific; 2004. p. 342–426.
23. Merrill DR, Bikson M, Jefferys JGR. Electrical stimulation of excitable tissue: design of efficacious and safe protocols. *J Neurosci Methods.* 2005 Feb 15;141(2):171–98.
24. Cogan SF. Neural stimulation and recording electrodes. *Annu Rev Biomed Eng.* 2008;10:275–309.
25. Vetter CP. Development towards improved durability of implanted neuroprosthetic electrodes through surface modifications. MS Thesis. Indianapolis, IN: Indiana University-Purdue University; 2020.
26. Lazorchak N, Horn MR, Yoshida K. Low frequency alternating current block-activation window: in-silico predictions. In: 25th Annual Meeting of the International Functional Electrical Stimulation Society at Rehabweek 2022. Rotterdam: International Functional Electrical Stimulation Society; 2022.
27. Rodriguez FJ, Ceballos D, Schüttler M, Valero A, Valderrama E, Stieglitz T, et al. Polyimide cuff electrodes for peripheral nerve stimulation. *J Neurosci Methods.* 2000 Jun;98(2):105–18.
28. Yu H, Xiong W, Zhang H, Wang W, Li Z. A Parylene self-locking cuff electrode for peripheral nerve stimulation and recording. *J Microelectromech Syst.* 2014 Oct;23(5):1025–35.
29. Richardson L, Ahmed C, Smolik M, Yoshida K. 3D printed hinged multi-contact cuff electrodes for rapid prototyping and testing. In: 22 Annual Conference of the International Functional Electrical Stimulation Society. Nottwil, Switzerland: International Functional Electrical Stimulation Society; 2018. p. 123–6.
30. Horn MR, Alhawwash A, Yoshida K. In-vivo measurement of the block activation window for sinusoidal low frequency alternating current (LFAC) stimulation. In: 2022 International Society for Electromyography and Kinesiology Congress. Québec City: International Society for Electromyography and Kinesiology Congress; 2022. p. 144.
31. Yoshida K, Mauser K, Stavnschoj J. Digitally invertible universal amplifier for recording and processing bioelectric signals. US Patent# 9.622.972B2, 2017.
32. Sempsrott D. Analysis of the bioelectric impedance of the tissue-electrode interface using a novel full-spectrum approach. MS Thesis. Indianapolis, IN: Purdue University; 2014.
33. `sigm_fit`. MathWorks; 2022. (MATLAB Central File Exchange).

How to cite this article: Doering OM, Vetter C, Alhawwash A, Horn MR & Yoshida K. Durable scalable 3D SLA-printed cuff electrodes with high performance carbon + PEDOT:PSS-based contacts. *Artif. Organs.* 2022;46:2073–2096. <https://doi.org/10.1111/aor.14387>